Published in final edited form as:

Immunity. 2016 July 19; 45(1): 145–158. doi:10.1016/j.immuni.2016.06.009.

Interleukin-13 activates distinct cellular pathways leading to ductular reaction, steatosis, and fibrosis

Richard L. Gieseck III[1,2], **Thirumalai R. Ramalingam**[1], **Kevin M. Hart**[1], **Kevin M. Vannella**[1], **David A. Cantu**[1], **Wei-Yu Lu**[3], **Sofía Ferreira-González**[3], **Stuart J. Forbes**[3], **Ludovic Vallier**[2,4], and **Thomas A. Wynn**[1,*]

[1]Immunopathogenesis Section, Laboratory of Parasitic Diseases, National Institute of Allergy and Infectious Diseases, National Institutes of Health, Bethesda, Maryland, 20852, USA

[2]Wellcome Trust–Medical Research Council Stem Cell Institute, Anne McLaren Laboratory, Department of Surgery, University of Cambridge, Cambridge, UK

[3]Medical Research Council Centre for Regenerative Medicine, University of Edinburgh, Edinburgh, UK

[4]Wellcome Trust Sanger Institute, Hinxton, UK

Summary

Fibroproliferative diseases are driven by dysregulated tissue repair responses and are major cause of morbidity and mortality as they affect nearly every organ system. Type-2 cytokine responses are critically involved in tissue repair; however, the mechanisms that regulate beneficial regeneration versus pathological fibrosis are not well understood. Here, we have shown that the type-2 effector cytokine interleukin-13 simultaneously, yet independently, directed hepatic fibrosis and the compensatory proliferation of hepatocytes and biliary cells in progressive models of liver disease induced by interleukin-13 over-expression or following infection with *Schistosoma mansoni*. Using transgenic mice with interleukin-13 signaling genetically disrupted in hepatocytes, cholangiocytes, or resident tissue fibroblasts, we have revealed direct and distinct roles for interleukin-13 in fibrosis, steatosis, cholestasis, and ductular reaction. Together, these studies show that these mechanisms are simultaneously controlled but distinctly regulated by interleukin-13 signaling. Thus, it may be possible to promote interleukin-13-dependent hepatobiliary expansion without generating pathological fibrosis.

Graphical Abstract

*Corresponding Author: twynn@niaid.nih.gov.

Author Contributions:

Experiments were conceived and designed by RG, TR, LV, and TW. Experiments were performed by RG, TR, KH, KV, DC, and TW. WL and SG conducted DAB-EpCAM staining and provided training for the isolation and culture of HPCs in SFs lab. SF provided *Krt19*^{cre}ERT/^{cre}ERT$_{Rosa26}$$^{tdTomato/tdTomato}$ mice and pathological expertise. RG performed IPA and statistical analyses. RG, TR, and TW wrote the manuscript.

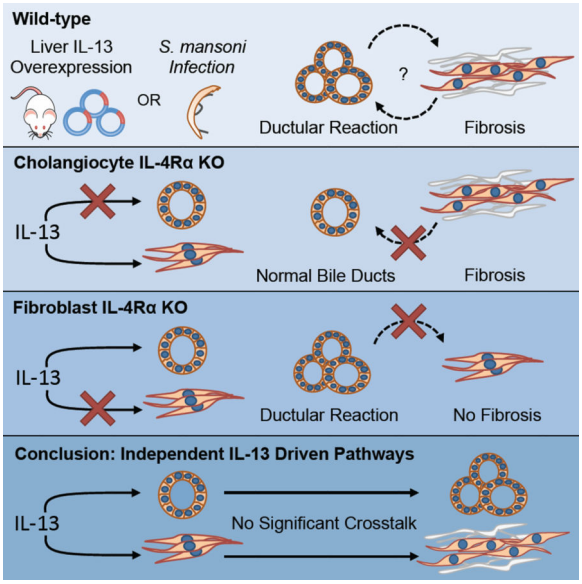

Introduction

The liver is remarkable in its ability to regenerate despite repeated injury. Different from many other organs which utilize stem cell populations to replace tissues, the liver relies heavily upon hepatocytes and cholangiocytes to exit quiescence and divide (Yanger et al., 2014). Recent studies have demonstrated distinct hepatocyte subsets, which contribute to hepatocyte turnover during homeostasis (Wang et al., 2015) and during mild chronic injury (Font-Burgada et al., 2015). However, during severe chronic injury, damaged hepatocytes can lose the ability to divide (Roskams, 2006), and in response, a population of putative hepatobiliary progenitor cells (HPCs) expands (Farber, 1956; Huch et al., 2015; Lu et al., 2015). Although several studies have questioned the source of HPCs and whether HPCs exhibit bipotent progenitor capacity (Jors et al., 2015), other recent studies have demonstrated that these cells can completely repopulate the liver following injuries that induce hepatocellular senescence (Lu et al., 2015). These differences in behavior and potency of HPCs may be explained by differences in the etiology of liver injury; nevertheless, it has been well established that the dysregulated signaling microenvironment of the injured liver can lead to aberrant proliferation of both HPCs and existing cholangiocytes (bile duct epithelial cells), together facilitating a disorganized expansion of bile ducts and recruitment of inflammatory cells known as ductular reaction (DR) (Roskams et al., 2004).

DRs are encountered in virtually every acute and chronic liver disorder in which there is organ-wide liver damage and cell loss. Proliferating ductules derived from HPCs or existing cholangiocytes may fail to drain bile contents properly, leading to local necrosis and progression towards cancers such as hepatocellular or cholangiocarcinoma (Alison and Lovell, 2005; Park et al., 2007). Furthermore, it has been well documented that the presence of DR is highly correlated with the progression of hepatic fibrosis and emergence of lipid abnormalities, although the mechanisms behind these correlations are debated and not well

understood (Clouston et al., 2005; Richardson et al., 2007). Thus, presence of DRs is an important prognostic marker of advanced liver disease, with patients exhibiting DRs generally having poor clinical outcomes (Lowes et al., 1999; Roskams, 2006; Sancho-Bru et al., 2012). Nevertheless, the signaling pathways governing these dysregulated responses remain unclear, limiting our ability to combat these severe complications in the clinic.

Interleukin-13 (IL-13) has been identified as a major pathogenic cytokine in helminth induced liver disease and several other chronic diseases associated with persistent type-2 cytokine production (Chiaramonte et al., 1999). Consequently, therapeutic antibodies targeting IL-13 signaling pathways are currently being investigated in several major clinical trials. Interestingly however, type-2 cytokine responses have also been linked with wound repair following acute tissue injury (Chen et al., 2012; Kaviratne et al., 2004). Nevertheless, the mechanisms that govern tissue regeneration versus pathological type-2 cytokine-driven fibrosis remain unclear. While previous studies have implicated M2 macrophages in repair and fibrosis (Borthwick et al., 2015; Chen et al., 2012), other cells including hepatocytes, cholangiocytes, HPCs, and fibroblasts also express functional IL-4 and IL-13 receptors, yet their roles in the progression of liver disease, steatosis, fibrosis, DR, and liver regeneration during chronic type-2 cytokine-driven inflammatory responses have remained unclear. Moreover, while clinical studies have found elevated type-2 cytokines and receptor expression in human patients with biliary atresia (Li et al., 2011), primary biliary cirrhosis, primary sclerosing cholangitis, hepatitis C infection, and autoimmune hepatitis (Landi et al., 2014), no previous studies have directly investigated the causal relationships between type-2 cytokine-driven fibrosis and DR. Therefore, we generated a series of cell-specific genetically ablated mice in which IL-4 receptor alpha chain (IL-4Rα), an essential receptor component for both IL-4 and IL-13 signaling, was targeted for deletion in biliary cells (defined as both HPCs and existing cholangiocytes), hepatocytes, and fibroblasts to elucidate the cellular pathways instructed by IL-13 that regulate the emergence of DRs and fibrosis during schistosomiasis, a disease affecting over 250 million individuals that induces a progressive liver fibrosis that manifests complications seen in advanced cirrhosis of many etiologies.

Results

IL-4 and/or IL-13 Signaling in Hepatocytes and/or Biliary Cells drive DR but not Fibrosis

Il4ra$^{flox/flox}$*Alb*$^{WT/cre}$ (*Alb-cre*$^{+}$) mice and *Il4ra*$^{flox/flox}$ (*Alb-cre*$^{-}$) littermates were studied over the course of an 18-week *S. mansoni* infection that results in progressive, type-2 cytokine-driven liver fibrosis. Due to expression of albumin by hepatoblasts (Sparks et al., 2010), the developmental precursor of both hepatocytes and cholangiocytes, these mice express cre-recombinase, and therefore have impaired IL-4Rα expression, in both hepatocytes and biliary cells. No significant differences in fibrosis were seen at 10 or 18 weeks as assessed by tissue hydroxyproline content (Figure 1A) and picrosirius red (PSR) staining (Figure 1B), ruling out a role for IL-4 and IL-13 signaling through IL-4Rα-expressing hepatocytes, cholangiocytes, or HPCs in the progression of fibrosis. Epithelial cell adhesion molecule (EpCAM) uniquely marks the biliary compartment within the liver, and by 10 weeks post-infection, significant expansion of EpCAM^{+} cells was evident around the granulomas of *Alb-cre*$^{-}$, but not *Alb-cre*$^{+}$ mice (Figure 1C upper panels, D). By 18

weeks, *Alb-cre*$^{-}$ mice exhibited abundant EpCAM^{+} ductules in the periphery of the granulomas, but the *Alb-cre*$^{+}$ group did not (Figure 1C lower panels, D,). Additionally, *Alb-cre*$^{-}$ mice exhibited significantly elevated liver weights compared to their *Alb-cre*$^{+}$ littermates (Figure 1E) in agreement with a recent study implicating IL-4 signaling with hepatocyte proliferation (Goh et al., 2013). Nearly 36% of EpCAM^{+} cells in *Alb-cre*$^{-}$ mice co-stained positive for Ki-67 indicating active proliferation in response to IL-4 and/or IL-13, compared to 2% in *Alb-cre*$^{+}$ littermates (Figure 1F, H). *Alb-cre*$^{-}$ mice also exhibited microvesicular steatosis as assessed by Oil Red O staining (ORO) in hepatocytes throughout the liver (Figure 1I), which was visually diminished in the *Alb-cre*$^{+}$ group. No significant differences were seen in serum ALT and AST levels (Figure 1G), survival (Figure S1A), and worm burden (Figure S1B), suggesting that differences in liver injury severity were not contributing to these changes. Together, these data demonstrate that IL-4 and/or IL-13 signaling through hepatocytes and/or biliary cells is necessary for the DR and steatosis associated with *S. mansoni* infection, but do not significantly affect fibrosis (Figure 1J).

IL-13 but not IL-4 is Necessary for DR during S. mansoni Infection

IL-4Rα is implicated in two distinct signaling pathways (Ramalingam et al., 2008). Type-I signaling is mediated solely by IL-4 following engagement of IL-4Rα:γ_c heterodimers by IL-4. Whereas type-II signaling is activated when either IL-4 or IL-13 engage IL-4Rα:IL-13Rα1 heterodimers. To determine if the DR seen in *Alb-cre*$^{-}$ but not in *Alb-cre*$^{+}$ littermates (Figure 2A, B, F) was mediated through type-I or type-II IL-4Rα signaling, we utilized an *Il13ra1*$^{-/-}$ model to selectively deplete type-II signaling. After 12 weeks of infection, no evidence of DR was seen, suggesting that type-II signaling is necessary for the development of *S. mansoni* driven DR (Figure 2C, F). Given that both IL-4 and IL-13 can signal through the type-II IL-4Rα signaling complex, we set out to determine if one of these cytokines plays a dominant role in the progression of DR or if either is sufficient. To this end, we utilized *Il4*$^{-/-}$ and *Il13*$^{-/-}$ mice to look for the presence of DR after the course of a 12-week infection. *Il4*$^{-/-}$ mice developed DR similar to wild type controls (Figure 2D, F); however, DR in *Il13*$^{-/-}$ mice was absent (Figure 2E, F), suggesting that IL-13 is the dominant type-2 cytokine in the progression of *S. mansoni* mediated DR (Figure 2G). Additionally, these mechanisms appear to operate independently of IL-33, which was recently found to promote extrahepatic, but not intrahepatic, ductal proliferation in experimental biliary atresia (Figure S2) (Li et al., 2014).

IL-13 Signaling in Hepatocytes and/or Biliary Cells Induces DR and Steatosis, but not Fibrosis

IL-13 has been identified as a key driver of pathology in a number of human diseases including idiopathic pulmonary fibrosis (Chandriani et al., 2014; Murray et al., 2014), asthma (Choy et al., 2015; Scheerens et al., 2014), atopic dermatitis (Metwally et al., 2004), and ulcerative colitis (Heller et al., 2005), among others. Consequently, several clinical trials have been completed or are underway testing the safety and efficacy of modulating IL-13 in these diseases (Beck et al., 2014; Brightling et al., 2015; Danese et al., 2015; Hamilton et al., 2014; Wenzel et al., 2013). In the previous section, we showed that DR required direct IL-13 signaling on hepatobiliary cells during the course of *S. mansoni* infection; however, helminth infections result in a complex immune response and an intercellular signaling

environment that evolves over time (Pearce and MacDonald, 2002). To determine the specific role of IL-13 directly and in the absence of other etiological agents, we designed an IL-13 overexpression plasmid (13-OP) and used hydrodynamic tail vein injection to induce overexpression within the liver (Liu et al., 1999). Quantitation of mRNA collected from liver 9 days post injection determined that 13-OP caused a significant upregulation of IL-13 mRNA and specific STAT6-inducible targets such as procollagen 6a (*Col6a1*) and interleukin-13 receptor alpha 2 (*Il13ra2*) without inducing *Il4* (Figure 3A). 13-OP induced a significant fibrotic response in both the *Alb-cre*$^{+}$ and *Alb-cre*$^{-}$ groups as assessed by tissue hydroxyproline content (Figure 3B) and PSR staining (Figure 3C), again ruling out a role for IL-13 signaling through IL-4Rα-expressing hepatocytes, cholangiocytes, or HPCs in the progression of fibrosis. EpCAM^{+} ductules in *Alb-cre*$^{-}$ mice were over 39% Ki-67^{+}, while little evidence of proliferation was observed in the *Alb-cre*$^{+}$ mice (Figure 3D, G). 13-OP also induced significant steatosis in the *Alb-cre*$^{-}$ mice but not in the *Alb-cre*$^{+}$ group (Figure 3E, H) that corresponded with increases in serum triglyceride levels in the *Alb-cre*$^{-}$ group (Figure 3F). No significant differences were seen in survival (Figure S3A) or serum ALT and AST levels (Figure S3B), once again suggesting that differences in injury severity are not underlying these changes.

Microarray analyses were performed on whole liver from the 13-OP mice and GFP-OP control groups to elucidate the signaling pathways being activated by IL-13 signaling in hepatocytes and biliary cells. Over 130 genes exhibited over a two-fold difference ($p < 0.01$) between the 13-OP *Alb-cre*$^{+}$ and *Alb-cre*$^{-}$ groups (Figure 3I). Key differences included the downregulation of the classical and acidic pathways of bile acid synthesis, induction of cellular senescence, metabolic switch to lipogenesis, and recruitment of type-2 cell immune mediators (Figure 3J, L), all of which were dependent on IL-13 signaling through IL-4Rα^{+} hepatocytes and/or biliary cells. Furthermore, Ingenuity Pathway Analysis (IPA) revealed the key mediators induced by IL-13 signaling in *Alb-cre*$^{-}$ mice that were not active in *Alb-cre*$^{+}$ littermates (Figure 3K). These data establish that IL-13 alone can directly recapitulate key aspects of *S. mansoni*-driven pathology including fibrosis, DR, and steatosis. Furthermore, mice with non-functional IL-4Rα in hepatocytes and biliary cells displayed markedly reduced DR and steatosis but developed normal fibrosis, confirming the critical role of IL-13 and IL-4Rα signaling in these cell types for development of DR and steatosis, further supporting the growing data demonstrating IL-13 as a key pathogenic agent in a variety of human diseases.

Direct IL-13 Signaling in Biliary Cells Induces DR and Steatosis, but not Fibrosis

Since the *Alb-cre* model induces recombination in both the hepatocyte and biliary compartments, we next utilized *Il4ra*$^{\text{flox/flox}}$*Krt19*$^{\text{WT/}cre\text{-ERT}}$ mice to restrict recombination to the adult biliary compartment (Means et al., 2008), allowing us to discern the distinct role of type-2 signaling in biliary cells. *Il4ra*$^{\text{flox/flox}}$*Krt19*$^{\text{WT/}cre\text{-ERT}}$ (*Krt19-cre*$^{+}$) and *Il4ra*$^{\text{flox/flox}}$ (*Krt19-cre*$^{-}$) littermates were administered tamoxifen diet for 3 weeks prior to 13-OP injection to induce deletion of the IL-4Rα-floxed segments in cholangiocytes and HPCs, but not hepatocytes. This administration regimen resulted in specific recombination in 95.1 ± 2.6% of EpCAM^{+} cells (Figure S4A, B). After 1 week, 13-OP induced a significant fibrotic response in both the *Krt19-cre*$^{+}$ and *Krt19-cre*$^{-}$ groups as evaluated by tissue

hydroxyproline content (Figure 4A), PSR staining (Figure 4B), and mRNA quantitation (Figure 4C), mirroring the results obtained with the *Alb-cre* expressing mice. EpCAM$^+$ ductules in *Krt19-cre*$^-$ mice, but not *Krt19-cre*$^+$, co-stained positive for Ki-67 expression, illustrating a direct and critical role for IL-13:IL-4Rα signaling in biliary cell proliferation (Figure 4D, E). Additionally, 13-OP induced severe steatosis in the *Krt19-cre*$^-$ mice but not the *Krt19-cre*$^+$ mice, suggesting that the upstream initiator of the steatosis seen in the *Alb-cre*$^-$ and *Krt19-cre*$^-$ mice is IL-13 signaling through the biliary compartment rather than through hepatocytes (Figure 4F, G). No significant differences were seen in survival (Figure S4C) and serum ALT and AST levels (Figure S4D) once again suggesting that differences in injury severity were not responsible for these changes.

To verify these results in an infectious setting, we subjected the *Krt19-cre* mice to a 12-week *S. mansoni* infection. Mice were administered tamoxifen diet during the course of infection to induce recombination. Similar to results from previous experiments using the *Alb-cre* models and the *Krt19-cre* 13-OP model, no significant differences in hydroxyproline content or PSR staining were observed between the two infected groups (Figure 4I, J). In contrast to the *Alb-cre* model, in which hepatocyte IL-4 and IL-13 signaling were disrupted, no differences in liver weight were observed between groups, again supporting previous work that has suggested that IL-4 acts directly on hepatocytes as a mitogen during injury (Goh et al., 2013) (Figure 4K). Similar to the other models, EpCAM$^+$ ductules in *Krt19-cre*$^-$ mice, but not *Krt19-cre*$^+$, co-stained positive for Ki-67 expression (Figure 4M, N). No significant differences in infection burden or serum ALT and AST were observed, ruling out that differences in DR are simply due to underlying differences in injury severity (Figure 4L, O). These data clearly establish that IL-13 signaling in biliary cells, not hepatocytes, results in DR and steatosis without affecting fibrosis (Figure 4H).

Since the *Krt19-cre* targets both cholangiocytes and HPCs in the adult liver, we next explored whether IL-13 could directly stimulate isolated HPCs. CD45$^-$ CD31$^-$ TER119$^-$ EpCAM$^+$ CD24$^+$CD133$^+$ HPCs (Lu et al., 2015) were isolated from the livers of *Il4Ra*$^{flox/flox}$ mice and stimulated with 50 ng/mL recombinant murine IL-13 or a vehicle control for 72 hours. IL-13 treatment caused cells to adopt a cuboidal shape with clearly defined cell boundaries (Figure S4E). Additionally, IL-13 treated cells proliferated more quickly than controls as assessed by Alamar blue reduction (Figure S4F). We employed microarray analysis to determine the pathways driven by IL-13 to establish the observed phenotype. More than 200 genes exhibited over 1.5-fold difference between the control and IL-13 treated groups (Figure S4G) including genes involved in Wnt and Notch signaling, key pathways in cholangiocyte differentiation, as well as immune cell trafficking and recruitment (Figure S4H). Taken together, these data suggest that IL-13 directs HPCs towards a cholangiocyte fate and recruits cells that have been shown to further contribute to cholangiocyte differentiation.

IL-13 Signaling through PDGFRB$^+$ Fibroblasts is Necessary for Type-2 Cytokine-Mediated Fibrosis

Next, to address the question of whether IL-13 signaling through fibroblasts is necessary for type-2 cytokine-driven fibrosis and/or DR, we utilized *Il4ra*$^{flox/flox}$ *Pdgfrb*$^{WT/cre}$ (*Pdgfrb-*

cre$^+$) mice to disrupt IL-13 signaling in liver resident tissue fibroblasts, also known as hepatic stellate cells (HSCs). Previous work has demonstrated that within the liver, the *Pdgfrb-cre* induces recombination specifically in HSCs and not in endothelium, macrophages, hepatocytes, cholangiocytes, or T cells (Henderson et al., 2013). Furthermore, we isolated HSCs from wild type and *Pdgfrb-cre*$^+$ mice and looked for the presence of native or recombined IL4Rα by genomic DNA genotyping and found efficiency of recombination approaching 100% (Figure S5A). We subjected these mice to 13-OP and GFP-OP injections and followed them for 7 days. *Pdgfrb-cre*$^+$ mice were significantly protected from fibrosis as assessed by tissue hydroxyproline content (Figure 5A) and PSR staining (Figure 5B), providing direct evidence that IL-13 signaling in PDGFRB$^+$ fibroblasts *in vivo* is critical for the development of fibrosis. mRNA expression showed significant upregulation of the fibrosis related transcripts *Col6a1* and *Postn* in the *Pdgfrb-cre*$^-$ group compared to *Pdgfrb-cre*$^+$ littermates (Figure 5C). Furthermore, *Pdgfrb-cre*$^+$ mice were significantly protected from mortality (S4B). Both groups exhibited marked microvesicular steatosis after 13-OP administration (Figure 5D). Despite the marked decrease in fibrosis and increased survival in the *Pdgfrb-cre*$^+$ mice, both 13-OP groups exhibited EpCAM$^+$Ki-67$^+$ DR (Figure 5E, Figure S5C), further illustrating that DR and fibrosis are distinctly and independently regulated by IL-13.

In order to validate these results in a chronic disease setting, *Pdgfrb-cre* mice were infected with *S. mansoni* and followed for 12 weeks. *Pdgfrb-cre*$^+$ mice were markedly protected from fibrosis as quantified by tissue hydroxyproline content (Figure 5F) and PSR staining (Figure 5G). Despite the significant differences in fibrosis, no significant differences were seen in survival through week 12 (Figure S5D). Quantitation of mRNA expression by qPCR revealed a stronger type-2 cytokine effector response in the *Pdgfrb-cre*$^+$ mice, likely due to the decreased expression of the neutralizing decoy receptor IL-13Rα2 by PDGFRB$^+$ fibroblasts (Figure S5F). Despite the significant decrease in fibrosis in the *Pdgfrb-cre*$^+$ mice, both groups exhibited extensive DR in the periphery of granulomas that co-stained EpCAM$^+$Ki-67$^+$ (Figure 5H, Figure S5E), clearly demonstrating that fibrosis and DR are independently regulated by IL-13 signaling through distinct cell types.

IL-13 Signaling in Hepatocytes and Fibroblasts Assists in the Recruitment of Eosinophils

Previous studies have identified eosinophils as a source of IL-13 during chronic liver injury (Reiman et al., 2006). In this study, we observed a significant role for hepatocytes and PDGFRB$^+$ fibroblasts in eotaxin-1 expression and the recruitment of eosinophils to the liver following type-2 cytokine-driven injury (Figure 6A–C). Although the results with *Krt19-cre*$^+$ mice revealed that IL-4Rα-expressing biliary cells had no significant role in eotaxin-1 expression or eosinophil recruitment, the close proximity of PDGFRB$^+$ periportal fibroblasts likely contributed to the marked accumulation eosinophils in areas surrounding bile ducts. Consequently, in addition to type 2 innate lymphoid cells (ILC2s) and T helper-2 (T_H2) cells, eosinophils recruited by IL-4Rα-expressing hepatocytes and fibroblasts likely serve as sources of IL-13, which reinforce myofibroblast activation and DR following injury (Figure 6D). As such, these findings reveal a link between hepatocytes, fibroblasts, and eosinophils in the development of fibrosis, DRs, and other pathologies of the liver.

IL-13 Driven DR Initiates Ductal Cholestasis Independently from Fibrosis

Cholestatic complications are a common feature of fibrotic liver diseases and can result in local necrosis and progression towards cancers such as hepatocellular or cholangiocarcinoma (Alison and Lovell, 2005; Park et al., 2007). Despite this, it is unknown whether cholestasis originates from stricture of bile ducts (obstructive cholestasis) or from other distinct mechanisms during the progression of IL-13-dependent fibrosis. In our various models of type-2 cytokine-driven liver damage, cholestasis was observed in the large branching ducts of *cre*- groups from each experiment, all of which exhibited both extensive fibrosis and DR (Figure 7A, B, C). *Alb-cre*$^{+}$ and *Krt19-cre*$^{+}$ mice, in which DR was eliminated but fibrosis was maintained, showed little evidence of cholesterol crystal precipitation, suggesting that excessive DR, rather than fibrosis, initiates cholestasis in response to IL-13 (Figure 7A, B). This hypothesis was further supported by the observation that *Pdgfrb-cre*$^{+}$ mice, in which fibrosis was reduced to levels of naïve animals but DR proceeds unimpeded, exhibited marked ductal cholestasis, as evidenced by the precipitation of cholesterol crystals in the large branching ducts (Figure 7C). Furthermore, in all mice exhibiting DR, bile ducts proliferated to the point of occluding the bile duct lumen (Figure 7D). Resin casting of the biliary tree in mice over-expressing IL-13 confirmed that these mice have strictures, presumably induced by excessive proliferation that results in a truncated biliary tree with many proliferative nodules, further supporting our hypothesis that excessive ductal proliferation rather than fibrosis results in cholestatic injury (Figure 7E, F). These discoveries emphasize that strategies utilizing type-2 cytokine driven repair and regeneration will need to be finely tuned and targeted to prevent these potentially serious complications.

Discussion

Some studies have suggested that IL-13 promotes fibrosis by increasing autocrine CTGF signaling in fibroblasts and by induction of the pro-fibrotic cytokine TGF-β1 via IL-13Rα2 signaling (Liu et al., 2011; Shimamura et al., 2008; Sugimoto et al., 2005). However, studies with neutralizing anti-TGF-β antibodies, soluble TGF-βR-Fc, and Tg mice (*Smad3*$^{-/-}$ and TGF-βRII-Fc), have suggested that IL-13 can induce fibrosis independently from TGF-β. *Il13ra2*$^{-/-}$ mice were also found to develop significantly worse IL-13 driven fibrosis than WT littermates, shedding further doubt on the importance of IL-13Rα2 triggered TGF-β1 expression (Chiaramonte et al., 2003). Instead, related studies have argued for a direct role for IL-4Rα:IL-13Rα1 triggered STAT6-signaling in the development of type-2 cytokine driven fibrosis (Wynn, 2015). However, whether IL-13 driven fibrosis is induced by direct targeting of fibroblasts *in vivo* or by other intermediate cell types and signaling mechanisms has remained unknown until this study. Here, we provide unequivocal evidence that IL-13 must engage fibroblasts directly to promote fibrosis and that disruption of this signaling pathway in PDGFRB^{+} HSCs is sufficient to reduce fibrosis to levels found in naïve animals. Furthermore, these studies establish that DR is completely uncoupled from fibrosis. During chronic type-2 cytokine-driven injury, circulating IL-13 directly targets both fibroblasts and biliary cells, resulting in the activation of ECM-producing myofibroblasts and concurrent DR, thus finally resolving the enigmatic correlation between DRs and fibrosis.

Together, these studies have revealed the distinct cell types targeted by IL-13 that concurrently drive hepatobiliary fibrosis, proliferation, steatosis, and associated pathologies. The duration and magnitude of the IL-13 response likely dictates whether the resulting repair response is adaptive or maladaptive. For example, in schistosomiasis, the fibrotic response initially encapsulates parasite eggs to prevent hepatocyte damage from cytotoxic egg antigens; however, during chronic infection, excessive accumulation of extracellular matrix components ultimately impedes blood flow, thus exacerbating damage.

Similarly, we have shown that IL-13 can act directly on bile duct epithelial cells (cholangiocytes) *in vivo* and promote HPC differentiation towards a cholangiocyte fate *in vitro*. During acute hepatic injury, local sources of IL-13 may assist in regeneration by prompting a transient proliferation of cholangiocytes to replace damaged ducts. However, in chronic cases where tissue-damaging irritants cannot be cleared, or during adaptive T_H2 cell-driven immune responses such as those present during chronic parasitic diseases, ductular proliferation can become maladaptive, predisposing to cholestatic complications as evidenced by the rapid occlusion of bile ducts and precipitation of cholesterol crystals within the large branching ducts.

The fact that steatosis was not seen in *Alb-cre*$^+$ and *Krt19-cre*$^+$ mice, which have impaired DR but normal fibrosis, but was present in *Pdgfrb-cre*$^+$ mice, which have extensive DR yet minimal fibrosis, supports the conclusion that steatosis is caused by IL-13-driven ductular occlusion rather than a result of severe fibrotic complications and fibrosis-driven ductal stricture. Furthermore, since steatosis failed to develop in both *Alb-cre*$^+$ (impaired IL-13 signaling through hepatocytes) and *Krt19-cre*$^+$ mice (normal IL-13 signaling in hepatocytes), one can rule out that cholestatic steatosis is induced by metabolic changes due to IL-13-driven STAT6 (Ricardo-Gonzalez et al., 2010) or IL-13-driven STAT3 (Stanya et al., 2013) signaling in hepatocytes as has been suggested previously. Instead, we posit that malabsorbtion of fat, due to lack of bile flow to the intestine secondary to IL-13 driven ductal occlusion, results in the induction of a lipogenic program within hepatocytes to compensate for lack of dietary fat, resulting in the steatotic appearance of hepatocytes in mice with DR. These findings are consistent with the steatosis that develops in rats during experimental bile duct ligation (Lin et al., 2011) and in human patients with extrahepatic cholestasis (Schaap et al., 2009). Indeed, our mice developed decreased glucokinase, decreased *Cyp7a1*, increased *Fgf21*, decreased glucose, and increased triglycerides, features commonly observed in patients with extrahepatic cholestasis.

We further hypothesize that the downregulation of the bile acid biosynthesis pathway may be part of a previously unappreciated feedback loop to mitigate the cholestatic damage ensuing from counterproductive DR. Surprisingly, we find no evidence of hepatocytic cholestasis despite the fact that we have ample evidence of obstructive cholestasis, likely due to the downregulation of bile acid synthesis secondary to bile duct occlusion. These data may explain the previously underappreciated link between ductular and lipid abnormalities that has been noted in patients with primary biliary cirrhosis (Sorrentino et al., 2010) and warrant further detailed investigation into the metabolic changes induced by IL-13-driven DR in the context of chronic fibrosis.

In summary, we have shown that IL-13 simultaneously, yet independently, directs fibrosis and hepatobiliary proliferation in both an infection induced and a sterile model of liver fibrosis. These IL-13-driven pathways likely represent an evolutionary response to preserve liver function during the course of chronic inflammatory liver disease. Nevertheless, during a relentless type-2 cytokine-driven disease, these regenerative responses quickly evolve into maladaptive processes as fibrosis and DRs accrue, and the associated steatosis and cholestasis worsen. It has been noted that between 80–90% of liver transplants experience major bile duct epithelium loss during the procedure, resulting in serious complications in up to 40% of patients (Karimian et al., 2013). Thus, these findings are of considerable interest to clinical and translational medicine because they reveal both the potential therapeutic and biomarker potential of IL-13 signaling in cholangiocyte differentiation and biliary regeneration and the potential risks associated with IL-13 modulation in the liver. Particularly, we believe the insights gained from this work demonstrating the possibility of decoupling the IL-13-driven proliferative processes from tissue fibrosis will be instrumental in developing cell-targeted therapies exploiting these specific pathways.

Experimental Procedures

Ethics Statement

The National Institute of Allergy and Infectious Diseases Division of Intramural Research Animal Care and Use Program, as part of the National Institutes of Health Intramural Research Program, approved all of the experimental procedures (protocol LPD 16E). The Program complies with all applicable provisions of the Animal Welfare Act (http://www.aphis.usda.gov/animal_welfare/downloads/awa/awa.pdf) and other federal statutes and regulations relating to animals.

Mice

Il4ra$^{flox/flox}$ mice were kindly provided by Dr. Frank Brombacher (University of Cape Town; Cape Town, South Africa). *Alb*$^{cre/cre}$ mice were purchased from Jackson Laboratories. *Krt19*^{cre}ERT/^{cre}ERTRosa26$^{tdTomato/tdTomato}$ mice were kindly provided by Prof. Stuart Forbes (University of Edinburgh, Edinburgh, UK) and were generated by Dr. Guoqiang Gu (Means et al., 2008). *Pdgfrb*$^{cre/cre}$ mice were kindly provided by Dr. Neil Henderson (University of Edinburgh, Edinburgh, UK) and were generated by Dr. Ralf Adams (Foo et al., 2006). *Il4*$^{-/-}$ mice were kindly provided by Dr. William E. Paul (NIAID, NIH). *Il13*$^{-/-}$ mice were kindly provided from Dr. Andrew Mckenzie (MRC Laboratory of Molecular Biology). *Il13ra1*$^{-/-}$ mice were kindly provided by Regeneron Pharmaceuticals Inc. (Tarrytown, NY). *Il33*$^{-/-}$ mice were kindly provided by Amgen Inc. (Seattle, WA).

All animals were housed under specific pathogen-free conditions at the National Institutes of Health in an American Association for the Accreditation of Laboratory Animal Care-approved facility. Experiments used littermates (both sexes) between 8–16 weeks of age unless otherwise noted.

S. Mansoni Infection

Mice were infected percutaneously by suspending tails in water containing 35 *S. mansoni* cercariae for 45 minutes. Cerceriae were obtained by shedding infected *Biomphalaria glabrata* snails (Biomedical Research Institute; Rockville, MD). At the time of euthanasia, livers were perfused to determine worm burden and were removed for subsequent analyses.

Plasmid Overexpression

IL-13 and eGFP overexpression plasmids were produced by GenScript USA Inc. (Piscataway, NJ) by ligating the ORFs for IL-13 (NM_008355) and eGFP into the multi-restriction site of a pRG977 vector (kindly provided by Regeneron Pharmaceuticals Inc.). Hydrodynamic delivery was performed as described previously (Liu et al., 1999).

Isolation of Murine Non-parenchymal Cell Fraction and Purification of HPCs

HPCs were isolated and cultured as has been described previously (Lu et al., 2015).

Histological Quantification

Quantification of EpCAM positivity and Ki-67 co-expression was conducted in ImageJ. An intensity filter was used to determine the percent positivity of at least 3, 20× views for each sample. Eosinophils stained with the Wright-Giemsa method and bile duct numbers were scored by a blinded pathologist. Blinding was achieved by covering group labels, randomizing slides, and replacing with labels with numbers. For *S. mansoni* infections, at least 5 granulomas were scored for each sample. For plasmid overexpression experiments, at least 5, 20× views were scored for each sample. ORO pixel percentage was quantified using Leica Aperio Scanscope Software.

Statistical Analyses

Prism 6 was used to compute statistical analyses. Two-tailed Welch's t-tests were used to determine statistical significance between the majority of samples. Samples with very large deviation between means (due to overexpression vectors) used Mann-Whitney U-tests to determine significance. Survival was compared using log-rank (Mantel-Cox) tests. Initial group sizes were estimated based on previous study variance and expected mortality. No statistical methods were used to predetermine sample size. Randomization during processing was achieved by processing mice according to cage (cre^- and cre^+ littermates were not separated). Mice were excluded from 13-OP studies if IL-13 overexpression was not detected by qPCR at time of euthanasia.

Microarrays

RNA isolated as described above was submitted to the NIAID Research Technologies Branch who performed microarray analyses using MouseWG-6 v2.0 and MouseRef-8 v2.0 arrays. Subsequent analyses were performed using TM4 MeV microarray software suite. Welch's t-tests were used to generate volcano plots ($p < 0.05$) from which list subsets were generated by using fold-difference cutoffs. Microarray data have been uploaded to the Gene Expression Omnibus (http://www.ncbi.nlm.nih.gov/geo/) with the accession numbers

GSE70704 and GSE70705. Fold change values were uploaded to Ingenuity Pathway Analysis (Qiagen) to determine potential upstream regulators.

Please refer to the Supplemental Experimental Procedures and Table S1 for additional in depth methods.

Supplementary Material

Refer to Web version on PubMed Central for supplementary material.

Acknowledgments

This research was supported by the Intramural Research Program of the National Institutes of Health, National Institute of Allergy and Infectious Disease. LV is funded by the ERC starting grant Relieve IMDs and the Cambridge Hospitals National Institute for Health Research Biomedical Research Center. The funders had no role in study design, data collection and analysis, decision to publish, or preparation of the manuscript. The authors declare no competing financial interests. We thank Frank Brombacher for sharing the IL-4Rα-floxed mice.

References

Alison MR, Lovell MJ. Liver cancer: the role of stem cells. Cell Prolif. 2005; 38:407–421. [PubMed: 16300653]

Beck LA, Thaci D, Hamilton JD, Graham NM, Bieber T, Rocklin R, Ming JE, Ren H, Kao R, Simpson E, et al. Dupilumab treatment in adults with moderate-to-severe atopic dermatitis. The New England journal of medicine. 2014; 371:130–139. [PubMed: 25006719]

Borthwick LA, Barron L, Hart KM, Vannella KM, Thompson RW, Oland S, Cheever A, Sciurba J, Ramalingam TR, Fisher AJ, Wynn TA. Macrophages are critical to the maintenance of IL-13-dependent lung inflammation and fibrosis. Mucosal immunology. 2015

Brightling CE, Chanez P, Leigh R, O'Byrne PM, Korn S, She D, May RD, Streicher K, Ranade K, Piper E. Efficacy and safety of tralokinumab in patients with severe uncontrolled asthma: a randomised, double-blind, placebo-controlled, phase 2b trial. The Lancet. Respiratory medicine. 2015; 3:692–701. [PubMed: 26231288]

Chandriani S, DePianto DJ, N'Diaye EN, Abbas AR, Jackman J, Bevers J, Ramirez-Carrozzi V, Pappu R, Kauder SE, Toy K, et al. Endogenously Expressed IL-13R alpha 2 Attenuates IL-13-Mediated Responses but Does Not Activate Signaling in Human Lung Fibroblasts. J Immunol. 2014; 193:111–119. [PubMed: 24879793]

Chen F, Liu Z, Wu W, Rozo C, Bowdridge S, Millman A, Van Rooijen N, Urban JF Jr, Wynn TA, Gause WC. An essential role for TH2-type responses in limiting acute tissue damage during experimental helminth infection. Nat Med. 2012; 18:260–266. [PubMed: 22245779]

Chiaramonte MG, Donaldson DD, Cheever AW, Wynn TA. An IL-13 inhibitor blocks the development of hepatic fibrosis during a T-helper type 2-dominated inflammatory response. Journal of Clinical Investigation. 1999; 104:777–785. [PubMed: 10491413]

Chiaramonte MG, Mentink-Kane M, Jacobson BA, Cheever AW, Whitters MJ, Goad MEP, Wong A, Collins M, Donaldson DD, Grusby MJ, Wynn TA. Regulation and function of the interleukin 13 receptor alpha 2 during a T helper cell type 2-dominant immune response. J Exp Med. 2003; 197:687–701. [PubMed: 12642601]

Choy DF, Hart KM, Borthwick LA, Shikotra A, Nagarkar DR, Siddiqui S, Jia GQ, Ohri CM, Doran E, Vannella KM, et al. T(H)2 and T(H)17 inflammatory pathways are reciprocally regulated in asthma. Sci Transl Med. 2015; 7

Clouston AD, Powell EE, Walsh MJ, Richardson MM, Demetris AJ, Jonsson JR. Fibrosis correlates with a ductular reaction in hepatitis C: roles of impaired replication, progenitor cells and steatosis. Hepatology (Baltimore, Md). 2005; 41:809–818.

Danese S, Rudzinski J, Brandt W, Dupas JL, Peyrin-Biroulet L, Bouhnik Y, Kleczkowski D, Uebel P, Lukas M, Knutsson M, et al. Tralokinumab for moderate-to-severe UC: a randomised, double-blind, placebo-controlled, phase IIa study. Gut. 2015; 64:243–249. [PubMed: 25304132]

Farber E. Similarities in the sequence of early histological changes induced in the liver of the rat by ethionine, 2-acetylamino-fluorene, and 3'-methyl-4-dimethylaminoazobenzene. Cancer Res. 1956; 16:142–148. [PubMed: 13293655]

Font-Burgada J, Shalapour S, Ramaswamy S, Hsueh B, Rossell D, Umemura A, Taniguchi K, Nakagawa H, Valasek MA, Ye L, et al. Hybrid Periportal Hepatocytes Regenerate the Injured Liver without Giving Rise to Cancer. Cell. 2015; 162:766–779. [PubMed: 26276631]

Foo SS, Turner CJ, Adams S, Compagni A, Aubyn D, Kogata N, Lindblom P, Shani M, Zicha D, Adams RH. Ephrin-B2 controls cell motility and adhesion during blood-vessel-wall assembly. Cell. 2006; 124:161–173. [PubMed: 16413489]

Goh YPS, Henderson NC, Heredia JE, Eagle AR, Odegaard JI, Lehwald N, Nguyen KD, Sheppard D, Mukundan L, Locksley RM, Chawla A. Eosinophils secrete IL-4 to facilitate liver regeneration. P Natl Acad Sci USA. 2013; 110:9914–9919.

Hamilton JD, Suarez-Farinas M, Dhingra N, Cardinale I, Li X, Kostic A, Ming JE, Radin AR, Krueger JG, Graham N, et al. Dupilumab improves the molecular signature in skin of patients with moderate-to-severe atopic dermatitis. The Journal of allergy and clinical immunology. 2014; 134:1293–1300. [PubMed: 25482871]

Heller F, Florian P, Bojarski C, Richter J, Christ M, Hillenbrand B, Mankertz J, Gitter AH, Burgel N, Fromm M, et al. Interleukin-13 is the key effector Th2 cytokine in ulcerative colitis that affects epithelial tight junctions, apoptosis, and cell restitution. Gastroenterology. 2005; 129:550–564. [PubMed: 16083712]

Henderson NC, Arnold TD, Katamura Y, Giacomini MM, Rodriguez JD, McCarty JH, Pellicoro A, Raschperger E, Betsholtz C, Ruminski PG, et al. Targeting of alpha(v) integrin identifies a core molecular pathway that regulates fibrosis in several organs. Nat Med. 2013; 19:1617–1624. [PubMed: 24216753]

Huch M, Gehart H, van Boxtel R, Hamer K, Blokzijl F, Verstegen MM, Ellis E, van Wenum M, Fuchs SA, de Ligt J, et al. Long-term culture of genome-stable bipotent stem cells from adult human liver. Cell. 2015; 160:299–312. [PubMed: 25533785]

Jors S, Jeliazkova P, Ringelhan M, Thalhammer J, Durl S, Ferrer J, Sander M, Heikenwalder M, Schmid RM, Siveke JT, Geisler F. Lineage fate of ductular reactions in liver injury and carcinogenesis. The Journal of clinical investigation. 2015

Karimian N, op den Dries S, Porte RJ. The origin of biliary strictures after liver transplantation: Is it the amount of epithelial injury or insufficient regeneration that counts? Journal of hepatology. 2013; 58:1065–1067. [PubMed: 23466306]

Kaviratne M, Hesse M, Leusink M, Cheever AW, Davies SJ, McKerrow JH, Wakefield LM, Letterio JJ, Wynn TA. IL-13 activates a mechanism of tissue fibrosis that is completely TGF-beta independent. Journal of immunology. 2004; 173:4020–4029.

Landi A, Weismuller TJ, Lankisch TO, Santer DM, Tyrrell DLJ, Manns MP, Houghton M. Differential Serum Levels of Eosinophilic Eotaxins in Primary Sclerosing Cholangitis, Primary Biliary Cirrhosis, and Autoimmune Hepatitis. J Interf Cytok Res. 2014; 34:204–214.

Li J, Bessho K, Shivakumar P, Mourya R, Mohanty SK, dos Santos JL, Miura IK, Porta G, Bezerra JA. Th2 signals induce epithelial injury in mice and are compatible with the biliary atresia phenotype. Journal of Clinical Investigation. 2011; 121:4244–4256. [PubMed: 22005305]

Li , Razumilava N, Gores GJ, Walters S, Mizuochi T, Mourya R, Bessho K, Wang YH, Glaser SS, Shivakumar P, Bezerra JA. Biliary repair and carcinogenesis are mediated by IL-33-dependent cholangiocyte proliferation. The Journal of clinical investigation. 2014; 124:3241–3251. [PubMed: 24892809]

Lin J, Lu FK, Zheng W, Xu SY, Tai DA, Yu H, Huang ZW. Assessment of liver steatosis and fibrosis in rats using integrated coherent anti-Stokes Raman scattering and multiphoton imaging technique. J Biomed Opt. 2011; 16

Liu F, Song YK, Liu D. Hydrodynamics-based transfection in animals by systemic administration of plasmid DNA. Gene Ther. 1999; 6:1258–1266. [PubMed: 10455434]

Liu Y, Meyer C, Muller A, Herweck F, Li Q, Mullenbach R, Mertens PR, Dooley S, Weng HL. IL-13 Induces Connective Tissue Growth Factor in Rat Hepatic Stellate Cells via TGF-beta-Independent Smad Signaling. J Immunol. 2011; 187:2814–2823. [PubMed: 21804025]

Lowes KN, Brennan BA, Yeoh GC, Olynyk JK. Oval cell numbers in human chronic liver diseases are directly related to disease severity. Am J Pathol. 1999; 154:537–541. [PubMed: 10027411]

Lu WY, Bird TG, Boulter L, Tsuchiya A, Cole AM, Hay T, Guest RV, Wojtacha D, Man TY, Mackinnon A, et al. Hepatic progenitor cells of biliary origin with liver repopulation capacity. Nat Cell Biol. 2015; 17:971–983. [PubMed: 26192438]

Means AL, Xu Y, Zhao A, Ray KC, Gu G. A CK19(CreERT) knockin mouse line allows for conditional DNA recombination in epithelial cells in multiple endodermal organs. Genesis. 2008; 46:318–323. [PubMed: 18543299]

Metwally SS, Mosaad YM, Abdel-Samee ER, El-Gayyar MA, Abdel-Aziz AM, El-Chennawi FA. IL-13 gene expression in patients with atopic dermatitis: relation to IgE level and to disease severity. The Egyptian journal of immunology / Egyptian Association of Immunologists. 2004; 11:171–177. [PubMed: 16734130]

Murray LA, Zhang HL, Oak SR, Coelho AL, Herath A, Flaherty KR, Lee J, Bell M, Knight DA, Martinez FJ, et al. Targeting Interleukin-13 with Tralokinumab Attenuates Lung Fibrosis and Epithelial Damage in a Humanized SCID Idiopathic Pulmonary Fibrosis Model. Am J Resp Cell Mol. 2014; 50:985–994.

Park YN, Kojiro M, Di Tommaso L, Dhillon AP, Kondo F, Nakano M, Sakamoto M, Theise ND, Roncalli M. Ductular reaction is helpful in defining early stromal invasion, small hepatocellular carcinomas, and dysplastic nodules. Cancer. 2007; 109:915–923. [PubMed: 17279586]

Pearce EJ, MacDonald AS. The immunobiology of schistosomiasis. Nat Rev Immunol. 2002; 2:499–511. [PubMed: 12094224]

Ramalingam TR, Pesce JT, Sheikh F, Cheever AW, Mentink-Kane MM, Wilson MS, Stevens S, Valenzuela DM, Murphy AJ, Yancopoulos GD, et al. Unique functions of the type II interleukin 4 receptor identified in mice lacking the interleukin 13 receptor alpha1 chain. Nat Immunol. 2008; 9:25–33. [PubMed: 18066066]

Reiman RM, Thompson RW, Feng CG, Hari D, Knight R, Cheever AW, Rosenberg HF, Wynn TA. Interleukin-5 (IL-5) augments the progression of liver fibrosis by regulating IL-13 activity. Infect Immun. 2006; 74:1471–1479. [PubMed: 16495517]

Ricardo-Gonzalez RR, Red Eagle A, Odegaard JI, Jouihan H, Morel CR, Heredia JE, Mukundan L, Wu D, Locksley RM, Chawla A. IL-4/STAT6 immune axis regulates peripheral nutrient metabolism and insulin sensitivity. Proc Natl Acad Sci U S A. 2010; 107:22617–22622. [PubMed: 21149710]

Richardson MM, Jonsson JR, Powell EE, Brunt EM, Neuschwander-Tetri BA, Bhathal PS, Dixon JB, Weltman MD, Tilg H, Moschen AR, et al. Progressive fibrosis in nonalcoholic steatohepatitis: association with altered regeneration and a ductular reaction. Gastroenterology. 2007; 133:80–90. [PubMed: 17631134]

Roskams T. Liver stem cells and their implication in hepatocellular and cholangiocarcinoma. Oncogene. 2006; 25:3818–3822. [PubMed: 16799623]

Roskams TA, Theise ND, Balabaud C, Bhagat G, Bhathal PS, Bioulac-Sage P, Brunt EM, Crawford JM, Crosby HA, Desmet V, et al. Nomenclature of the finer branches of the biliary tree: canals, ductules, and ductular reactions in human livers. Hepatology (Baltimore, Md). 2004; 39:1739–1745.

Sancho-Bru P, Altamirano J, Rodrigo-Torres D, Coll M, Millan C, Lozano JJ, Miquel R, Arroyo V, Caballeria J, Gines P, Bataller R. Liver progenitor cell markers correlate with liver damage and predict short-term mortality in patients with alcoholic hepatitis. Hepatology. 2012; 55:1931–1941. [PubMed: 22278680]

Schaap FG, van der Gaag NA, Gouma DJ, Jansen PL. High expression of the bile salt-homeostatic hormone fibroblast growth factor 19 in the liver of patients with extrahepatic cholestasis. Hepatology. 2009; 49:1228–1235. [PubMed: 19185005]

Scheerens H, Arron JR, Zheng Y, Putnam WS, Erickson RW, Choy DF, Harris JM, Lee J, Jarjour NN, Matthews JG. The effects of lebrikizumab in patients with mild asthma following whole lung allergen challenge. Clin Exp Allergy. 2014; 44:38–46. [PubMed: 24131304]

Shimamura T, Fujisawa T, Husain SR, Kioi M, Nakajima A, Puri RK. Novel role of IL-13 in fibrosis induced by nonalcoholic steatohepatitis and its amelioration by IL-13R-directed cytotoxin in a rat model. J Immunol. 2008; 181:4656–4665. [PubMed: 18802068]

Sorrentino P, Terracciano L, D'Angelo S, Ferbo U, Bracigliano A, Tarantino L, Perrella A, Perrella O, De Chiara G, Panico L, et al. Oxidative stress and steatosis are cofactors of liver injury in primary biliary cirrhosis. Journal of gastroenterology. 2010; 45:1053–1062. [PubMed: 20393861]

Sparks EE, Huppert KA, Brown MA, Washington MK, Huppert SS. Notch Signaling Regulates Formation of the Three-Dimensional Architecture of Intrahepatic Bile Ducts in Mice. Hepatology. 2010; 51:1391–1400. [PubMed: 20069650]

Stanya KJ, Jacobi D, Liu S, Bhargava P, Dai L, Gangl MR, Inouye K, Barlow JL, Ji Y, Mizgerd JP, et al. Direct control of hepatic glucose production by interleukin-13 in mice. J Clin Invest. 2013; 123:261–271. [PubMed: 23257358]

Sugimoto R, Enjoji M, Nakamuta M, Ohta S, Kohjima M, Fukushima M, Kuniyoshi M, Arimura E, Morizono S, Kotoh K, Nawata H. Effect of IL-4 and IL-13 on collagen production in cultured LI90 human hepatic stellate cells. Liver Int. 2005; 25:420–428. [PubMed: 15780068]

Wang B, Zhao LD, Fish M, Logan CY, Nusse R. Self-renewing diploid Axin2(+) cells fuel homeostatic renewal of the liver. Nature. 2015; 524:180-+. [PubMed: 26245375]

Wenzel S, Ford L, Pearlman D, Spector S, Sher L, Skobieranda F, Wang L, Kirkesseli S, Rocklin R, Bock B, et al. Dupilumab in persistent asthma with elevated eosinophil levels. The New England journal of medicine. 2013; 368:2455–2466. [PubMed: 23688323]

Wynn TA. Type 2 cytokines: mechanisms and therapeutic strategies. Nat Rev Immunol. 2015; 15:271–282. [PubMed: 25882242]

Yanger K, Knigin D, Zong Y, Maggs L, Gu G, Akiyama H, Pikarsky E, Stanger BZ. Adult hepatocytes are generated by self-duplication rather than stem cell differentiation. Cell Stem Cell. 2014; 15:340–349. [PubMed: 25130492]

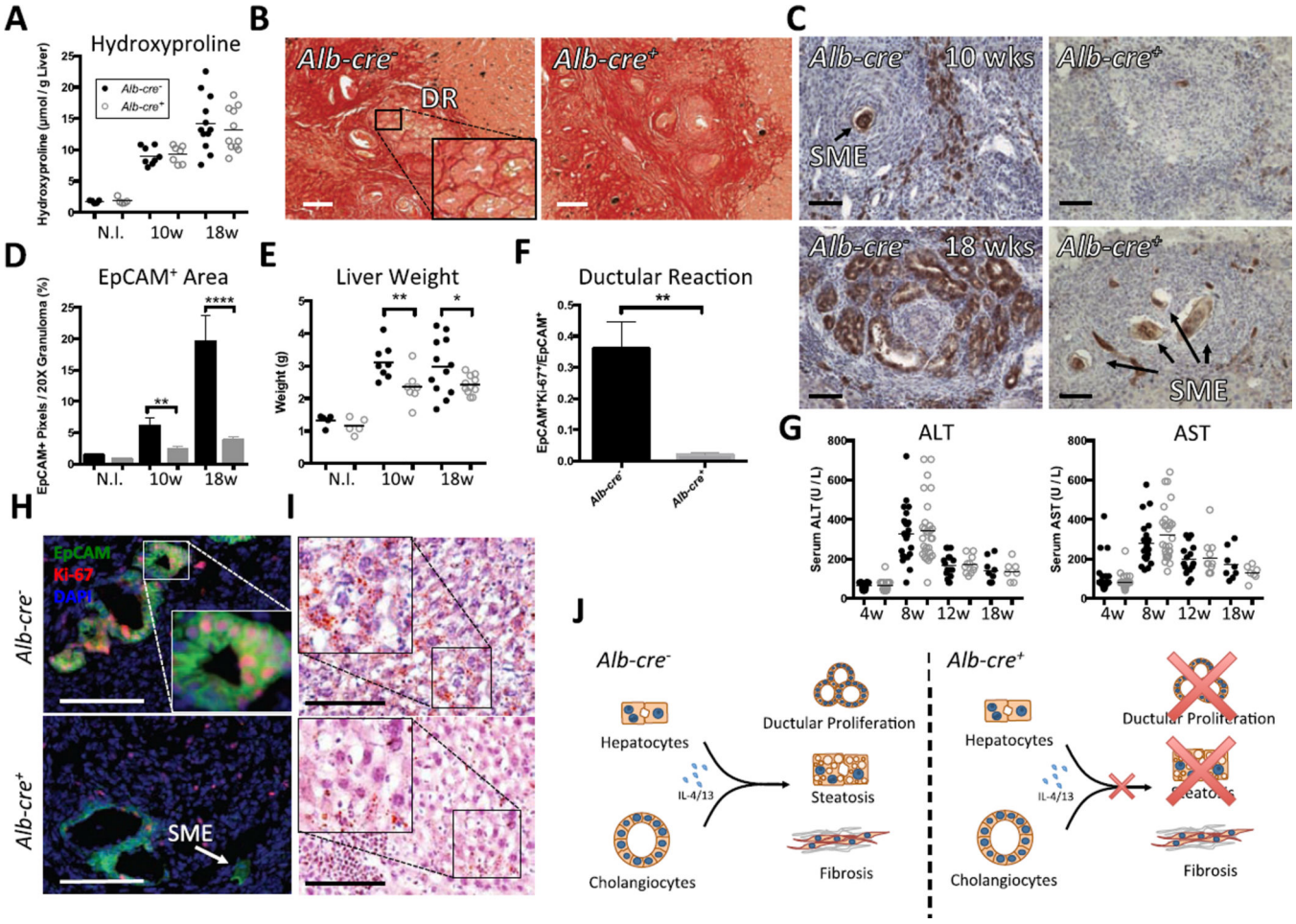

Figure 1. IL-4 and/or IL-13 Signaling in Hepatocytes and/or Biliary Cells Drive DR

(**A**) Hydroxyproline quantitation of naïve mice and mice infected with *S. mansoni* for 10 or 18 weeks. N-values left to right: n = 5, 5, 8, 7, 12, 11. (**B**) Picrosirius red (PSR) stain in mice infected for 18 weeks. (**C**) DAB-EpCAM immunohistochemistry of mice infected for 10 and 18 weeks highlighting peri-granuloma DR. (**D**) Quantitation of $EpCAM^+$ pixels per randomly chosen 20× microscopic field view. N-values left to right: n = 9, 9, 11, 15, 10, 14. (**E**) Quantitation of liver weights of naïve mice and mice infected for 10 or 18 weeks. N-values left to right: n = 5, 5, 8, 7, 12, 11. (**F**) Quantitation of DR as assessed by percentage of $EpCAM^+$ cells per randomly chosen 20× microscopic field view co-expressing Ki-67 at 18 weeks. N-values left to right: n = 9, 9. (**G**) Quantification of serum alanine transaminase (ALT) and aspartate transaminase (AST). N-values left to right: n = 40, 41, 24, 29, 16, 11, 9, 7. (**H**) Ki-67 and EpCAM immunostaining with DAPI nuclear counterstain of mice infected for 18 weeks. (**I**) ORO staining highlighting microvesicular lipid droplets after 18 weeks. (**J**) *Alb-cre*$^-$ animals exhibit DR, steatosis, and fibrosis after infection with *S. mansoni*. In contrast, *Alb-cre*$^+$ animals, in which IL-4 and IL-13 signaling is blocked in hepatocytes and cholangiocytes, do not develop significant DR or steatosis yet still have significant fibrosis. (Note) Results representative of three replicate experiments; All scale bars 100 μm; SME: non-specific staining due of *S. mansoni* eggs; DR: Ductular Reaction; results reported as mean ± S.E.M.; p*<0.05, p**<0.01, p***<0.001, p****<0.000; Please also see Figure S1.

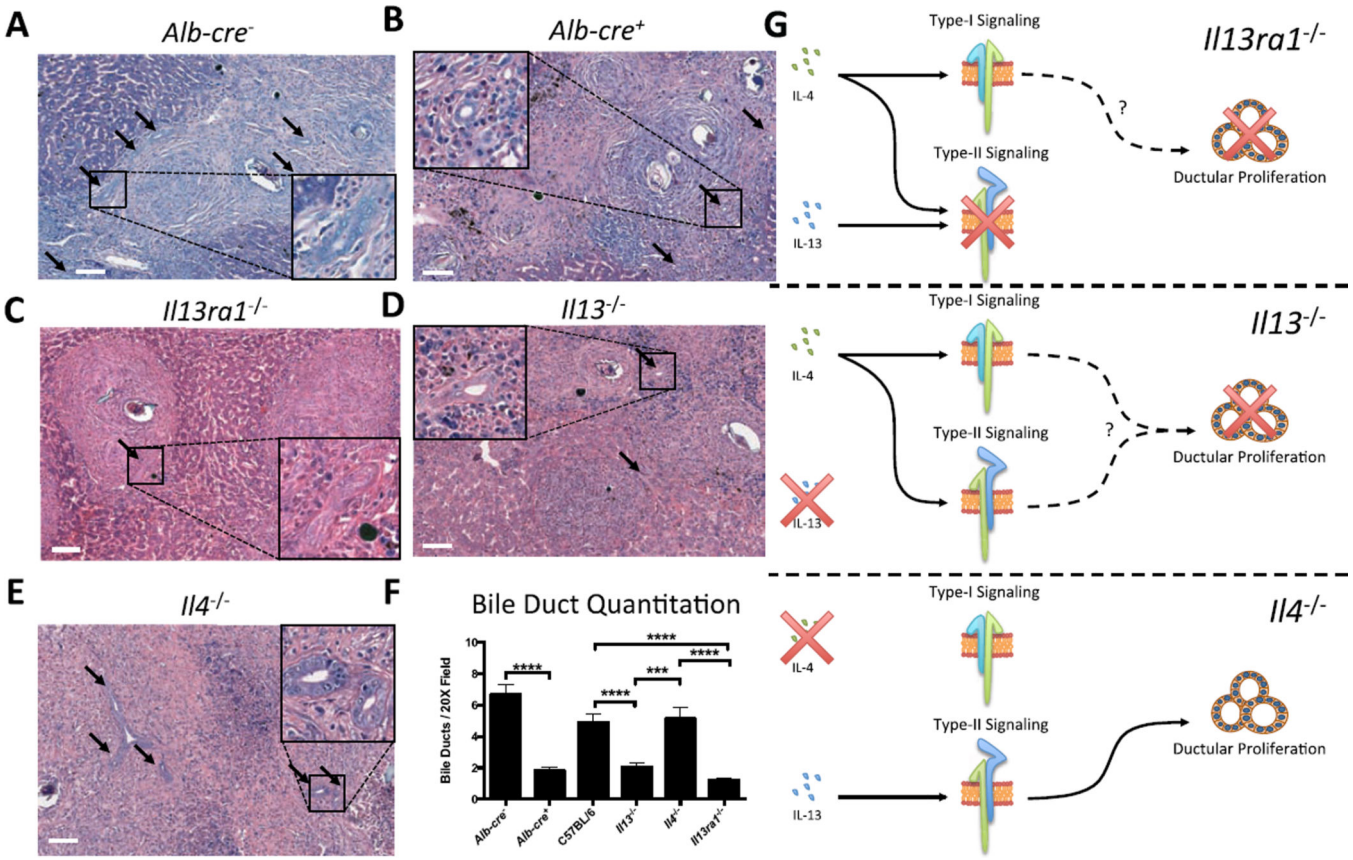

Figure 2. IL-13 is Necessary for DR during S. Mansoni Infection

Wright-Giemsa staining of 18-week infected (**A**) *Alb-cre*$^{-}$ and (**B**) *Alb-cre*$^{-}$ mice, and 12-week infected (**C**) *Il13ra1*$^{-/-}$, (**D**) *Il13*$^{-/-}$, (**E**) *Il4*$^{-/-}$ mice highlighting bile ducts. (**F**) Quantitation of number of bile ducts pixels per randomly chosen 20× microscopic field view. N-values left to right: n = 35, 40, 70, 40, 15, 75. Data is presented as mean ± SEM of at least 5 fields per mouse from at least 3 mice per group. (**G**) Schematic illustrating the signaling pathways blocked and active in each of the genetically ablated models. *Il13ra1*$^{-/-}$ mice, in which all IL-13 signaling is blocked and IL-4 can only signal through the type-1 receptor complex, fail to develop DR, demonstrating that the type-1 receptor is not involved in DR. Similarly, *Il13*$^{-/-}$ mice, in which IL- 4 signaling is normal, fail to develop DR, demonstrating that IL-4 is not involved in DR. However, *Il4*$^{-/-}$ mice, in which IL-13 signaling is normal, develop florid DRs, suggesting a crucial role for IL-13 in the pathogenesis of DR. (Note) Results representative of three replicate experiments. All scale bars 100 μm; Arrows highlight bile ducts; p*<0.05, p**<0.01, p***<0.001, p****<0.0001; please also see Figure S2.

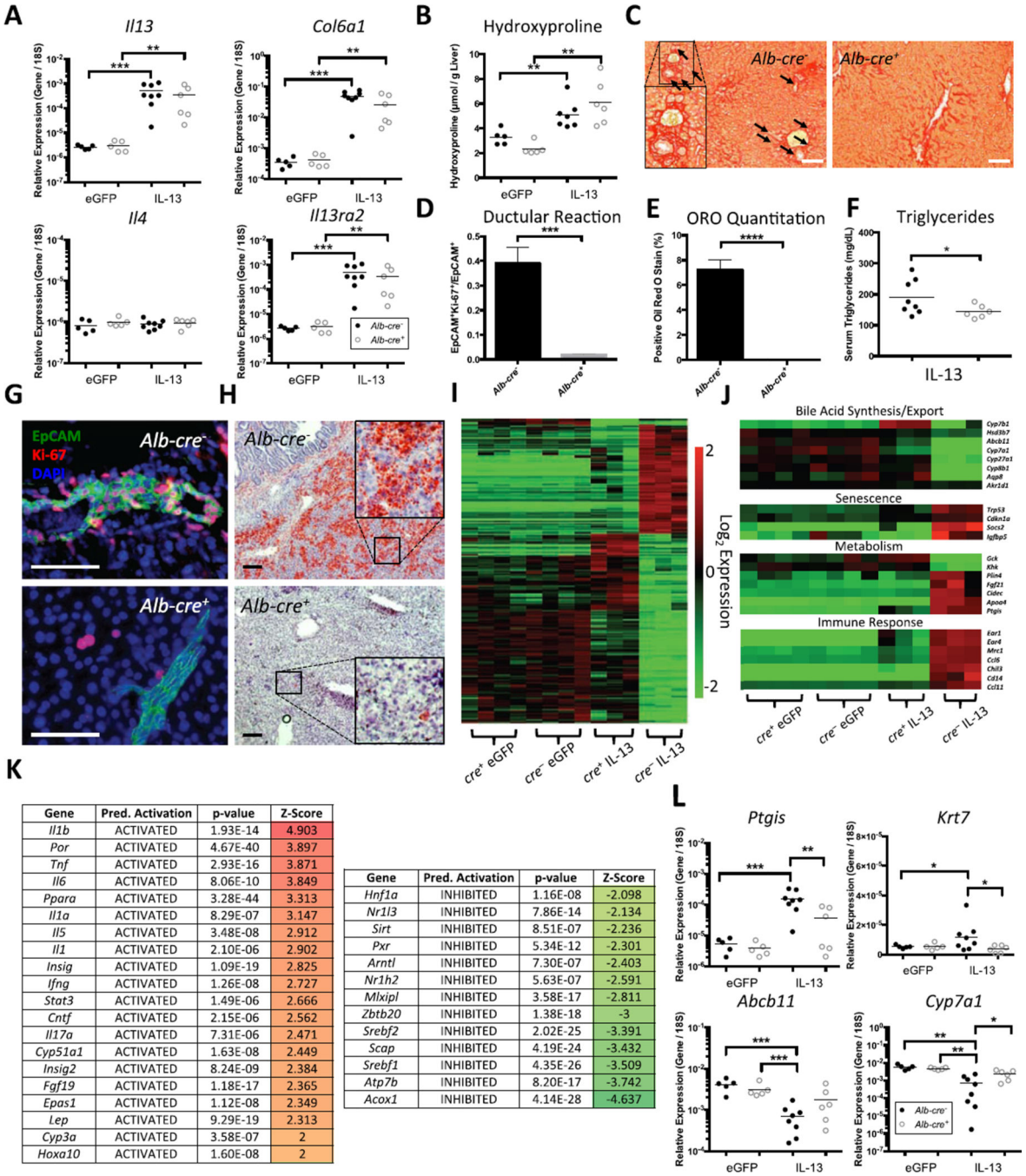

Gene	Pred. Activation	p-value	Z-Score
Il1b	ACTIVATED	1.93E-14	4.903
Por	ACTIVATED	4.67E-40	3.897
Tnf	ACTIVATED	2.93E-16	3.871
Il6	ACTIVATED	8.06E-10	3.849
Ppara	ACTIVATED	3.28E-44	3.313
Il1a	ACTIVATED	8.29E-07	3.147
Il5	ACTIVATED	3.48E-08	2.912
Il1	ACTIVATED	2.10E-06	2.902
Insig	ACTIVATED	1.09E-19	2.825
Ifng	ACTIVATED	1.26E-08	2.727
Stat3	ACTIVATED	1.49E-06	2.666
Cntf	ACTIVATED	2.15E-06	2.562
Il17a	ACTIVATED	7.31E-06	2.471
Cyp51a1	ACTIVATED	1.63E-08	2.449
Insig2	ACTIVATED	8.24E-09	2.384
Fgf19	ACTIVATED	1.18E-17	2.365
Epas1	ACTIVATED	1.12E-08	2.349
Lep	ACTIVATED	9.29E-19	2.313
Cyp3a	ACTIVATED	3.58E-07	2
Hoxa10	ACTIVATED	1.60E-08	2

Gene	Pred. Activation	p-value	Z-Score
Hnf1a	INHIBITED	1.16E-08	-2.098
Nr1i3	INHIBITED	7.86E-14	-2.134
Sirt	INHIBITED	8.51E-07	-2.236
Pxr	INHIBITED	5.34E-12	-2.301
Arntl	INHIBITED	7.30E-07	-2.403
Nr1h2	INHIBITED	5.63E-07	-2.591
Mlxipl	INHIBITED	3.58E-17	-2.811
Zbtb20	INHIBITED	1.38E-18	-3
Srebf2	INHIBITED	2.02E-25	-3.391
Scap	INHIBITED	4.19E-24	-3.432
Srebf1	INHIBITED	4.35E-26	-3.509
Atp7b	INHIBITED	8.20E-17	-3.742
Acox1	INHIBITED	4.14E-28	-4.637

Figure 3. IL-13 Signaling in Hepatocytes and/or Biliary Cells Induces DR

(**A**) Quantitation of mRNA expression by qPCR of IL-13 responsive genes relative to *18S* of mice injected with an eGFP or IL-13 overexpression plasmid after 9 days. N-values left to right: n = 5, 5, 8, 6. (**B**) Assessment of collagen deposition by hydroxyproline quantitation. N-values left to right: n = 5, 5, 8, 6. (**C**) PSR staining visualizing fibrotic deposition. (**D**) Quantitation of DR as percentage of EpCAM^{+} cells per randomly chosen 20× microscopic field view co-expressing Ki-67. N-values left to right: n = 9, 9. (**E**) Quantitation of percentage of ORO strong positive pixels per randomly selected 20× view. N-values left to

right: n = 9, 9. (**F**) Quantification of serum triglycerides taken at the time of euthanasia. N-values left to right: n = 8, 6. (**G**) Ki-67 and EpCAM immunostaining with DAPI nuclear counterstain of IL-13 overexpression mice. (**H**) ORO staining highlighting steatotic lipid droplets of IL-13 overexpression mice. (**I**) Subset of Illumina Beadchip microarray analysis showing genes selected using the following criteria: $p < 0.01$ (Welch's t-test, *Alb-cre*$^{+}$ IL-13 v. *Alb-cre*$^{-}$ IL-13), |Fold Difference| > 2 (*Alb-cre*$^{+}$ IL-13 v. *Alb-cre*$^{-}$ IL-13). (**J**) Select pathways significantly perturbed by IL-13 signaling through Alb^{+} cells ($p < 0.01$). (**K**) Ingenuity Pathway Analysis was utilized to identify differences in key downstream downstream mediators of metabolism, senescence, and bile acid synthesis in the *Alb-cre*$^{-}$ mice compared to the *Alb-cre*$^{+}$ mice. (**L**) Quantitation of mRNA expression by qPCR of select metabolism, bile synthesis, excretion, and inflammation-related genes identified by microarray analysis. N-values left to right: n = 5, 5, 8, 6. (Note) Data representative of two replicate experiments reported as mean ± S.E.M.; All scale bars 100 μm; Arrows point to bile ducts; p*<0.05, p**<0.01, p***<0.001, p****<0.0001; Please also see Figure S3.

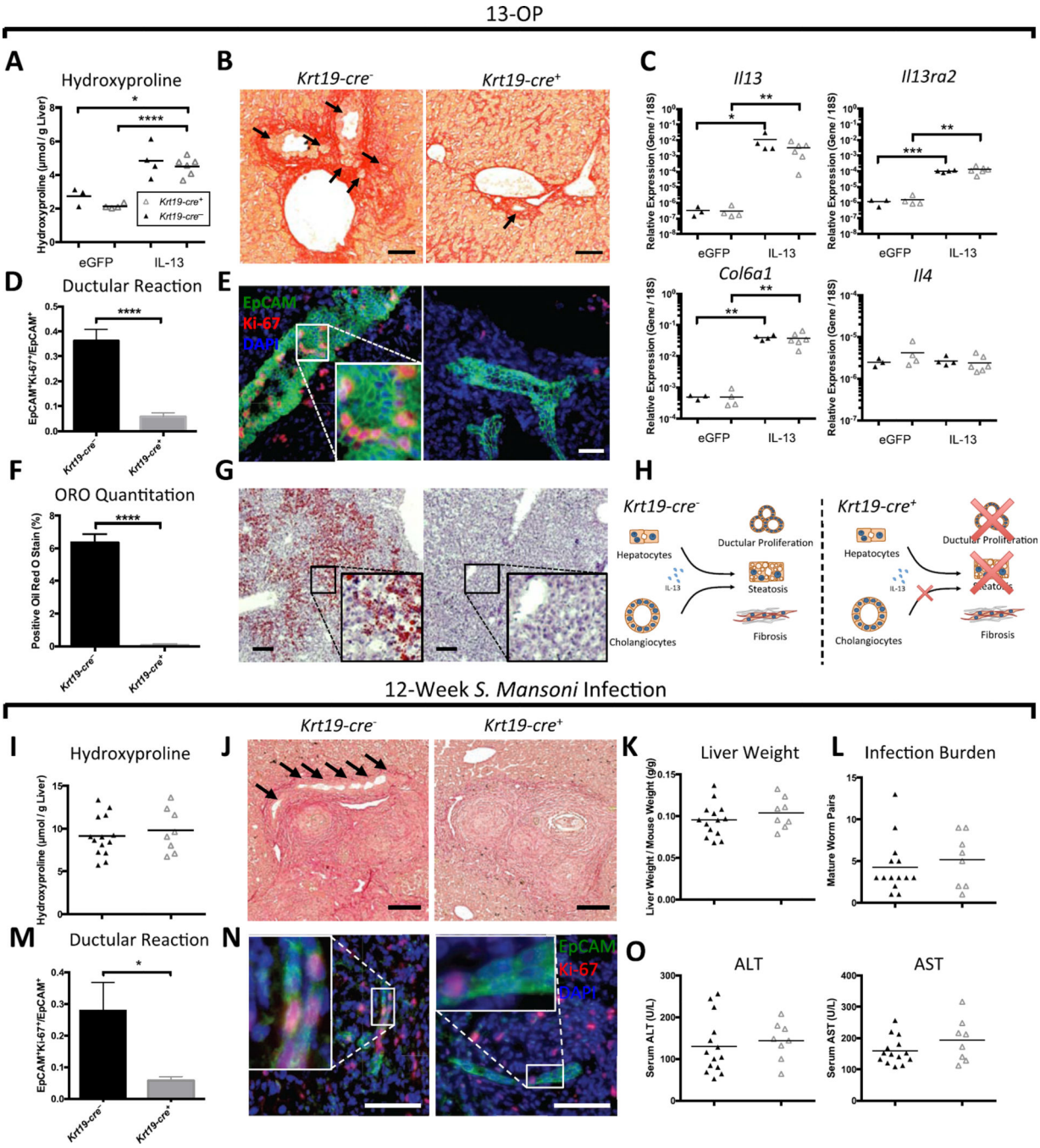

Figure 4. Direct IL-13 Signaling in Krt19^{+} Cells Induces DR and Steatosis

(**A**) Hydroxyproline quantitation of mice injected with an eGFP or IL-13 overexpression plasmid after 1 week. N-values left to right: n = 3, 4, 4, 6. (**B**) PSR staining visualizing quality of fibrotic deposition. (**C**) Quantitation of mRNA expression by qPCR of IL-13 responsive genes relative to *18S*. N-values left to right: n = 3, 4, 4, 6. (**D**) Quantitation of DR as assessed by percentage of EpCAM^{+} cells per randomly chosen 20× microscopic field view co-expressing Ki-67. N-values left to right: n = 9, 9. (**E**) Ki-67 and EpCAM immunostaining with DAPI nuclear counterstain of IL-13 overexpression mice. (**F**)

Quantitation of percentage of ORO strong positive pixels per randomly selected 20× view. N-values left to right: n = 9, 9. (**G) ORO** staining highlighting steatotic lipid droplets of IL-13 overexpression mice after 9 days. (**H**) *Krt19-cre*$^{-}$ animals exhibit DR, steatosis, and fibrosis after 13-OP. In contrast, *Krt19-cre*$^{+}$ animals, in which IL-13 signaling is blocked in cholangiocytes, but not hepatocytes and other cells, do not develop significant DR or steatosis, yet still have significant fibrosis. (**I**) Hydroxyproline quantitation of infected with *S. mansoni* for 12 weeks. N-values left to right: n = 14, 8. (**J**) PSR staining visualizing quality of fibrotic deposition. (**K**) Quantitation of liver weights of mice infected for 12 weeks. N-values left to right: n = 14, 8. (**L**) Infection Burden as assessed by number of mature worm pairs recovered after perfusion of the liver at time of euthanasia. N-values left to right: n = 14, 8. (**M**) Quantitation of DR as assessed by percentage of EpCAM^{+} cells per randomly chosen 20× microscopic field view co-expressing Ki-67. N-values left to right: n = 8, 10. (**N**) Ki-67 and EpCAM immunostaining with DAPI nuclear counterstain of infected mice. (**O**) Quantification of serum alanine transaminase (ALT) and aspartate transaminase (AST) obtained at the time of euthanasia. N-values left to right: n = 14, 8. (Note) Data representative of two replicate experiments; All scale bars 100 μm; Arrows point to bile ducts; p*<0.05, p**<0.01, p***<0.001, p****<0.0001; Please also see Figure S4.

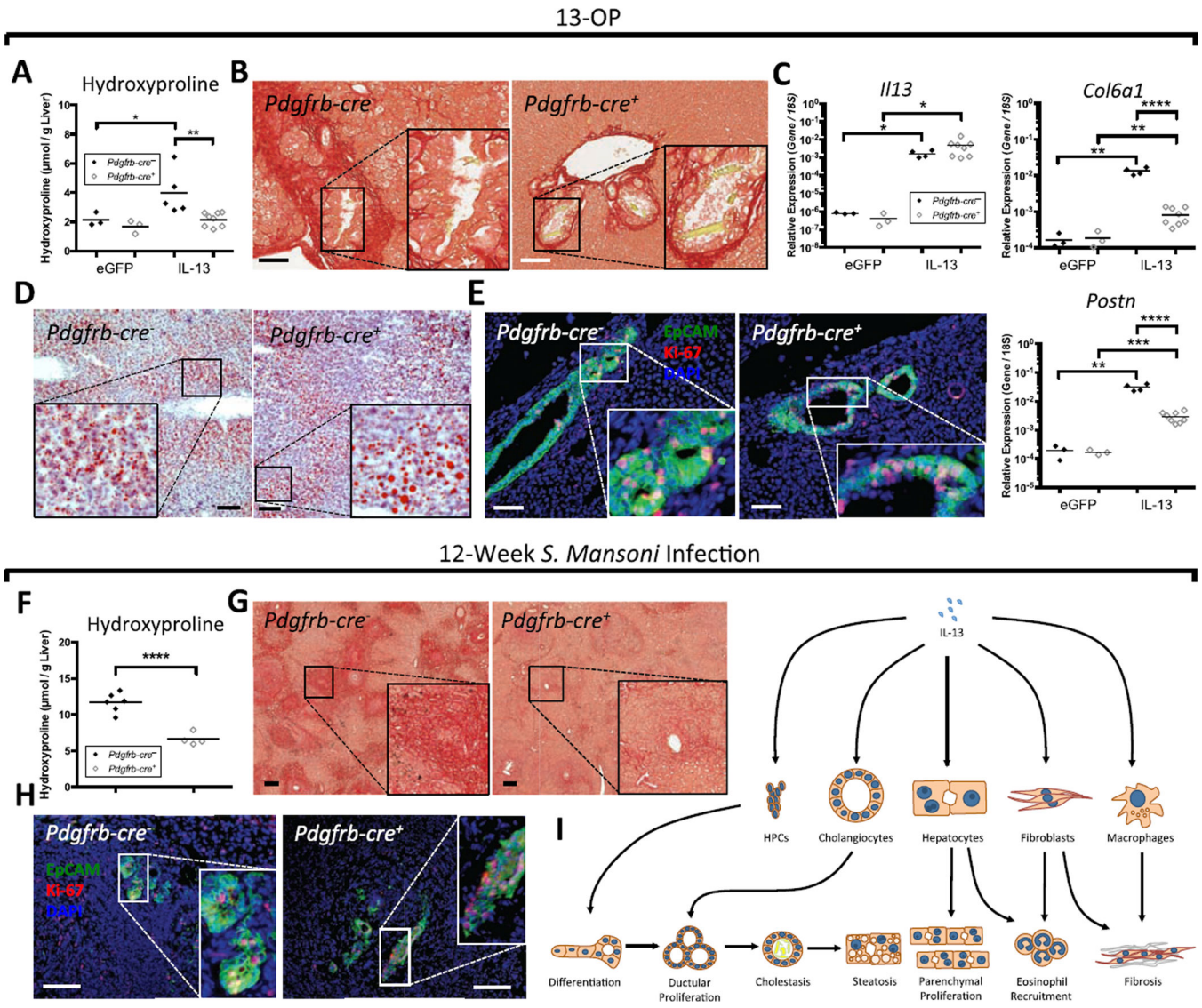

Figure 5. IL-13 Signaling through PDGFRB^{+} Fibroblasts is Necessary for IL-13 Driven Fibrosis

(**A**) Hydroxyproline quantitation of mice injected with an eGFP or IL-13 overexpression plasmid after 1 week. N-values left to right: n = 3, 3, 4, 8. (**B**) PSR staining visualizing fibrotic deposition. (**C**) Quantitation of mRNA expression by qPCR of IL-13 responsive genes relative to *18S*. N-values left to right: n = 3, 3, 4, 8. (**D**) ORO staining highlighting steatotic lipid droplets of IL-13 overexpression mice after 9 days. (**E**) Ki-67 and EpCAM immunostaining with DAPI nuclear counterstain of IL-13 overexpression mice highlighting DR. (**F**) Hydroxyproline quantitation of mice infected with *S. mansoni* for 12 weeks. N-values left to right: n = 6, 4. (**G**) PSR staining in mice infected for 12 weeks. (**H**) Ki-67 and EpCAM immunostaining with DAPI nuclear counterstain of mice infected for 12 weeks. (**I**) Schematic illustrating the different cell types targeted by IL-13 and downstream phenomenon related to each cell type. (Note) *S. mansoni* data representative of two replicate experiments; All scale bars 100 μm; p*<0.05, p**<0.01, p***<0.001, p****<0.0001; Please also see Figure S5.

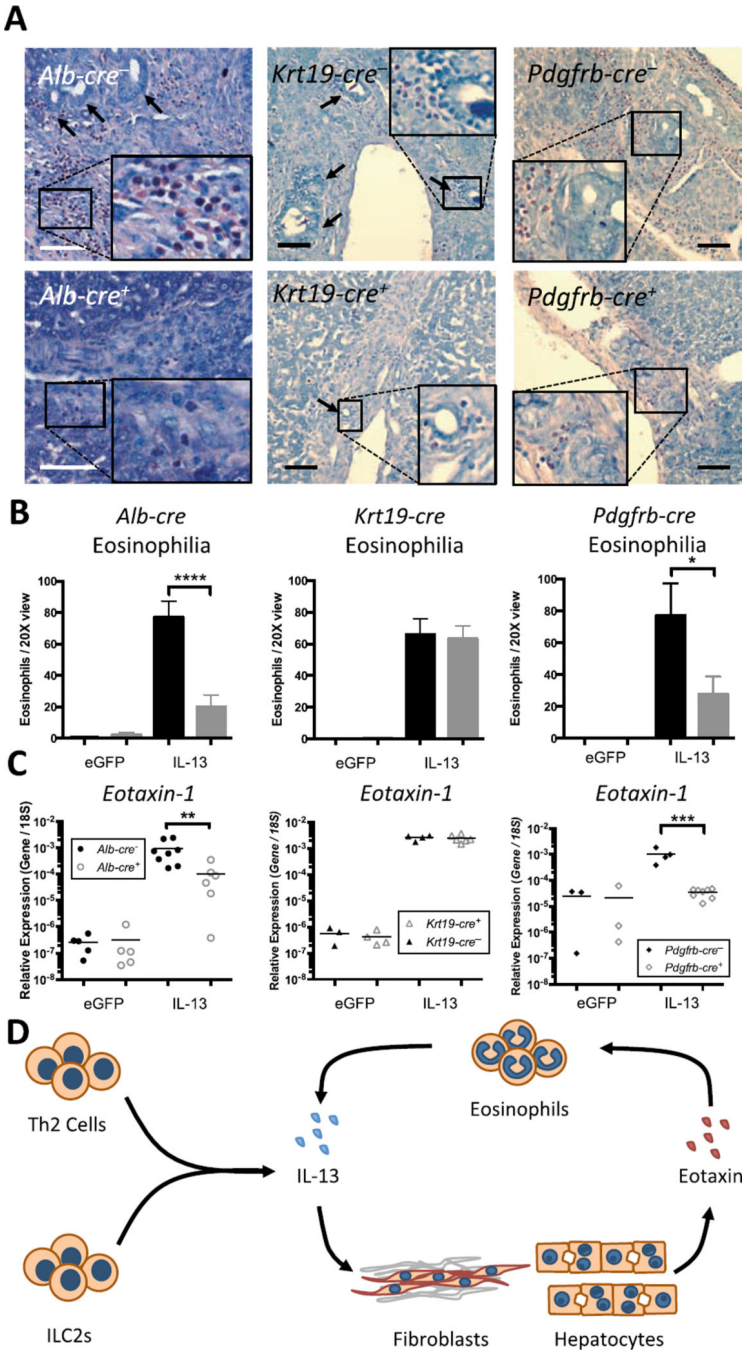

Figure 6. IL-13 Signaling in Hepatocytes and Fibroblasts Assists in the Recruitment of Eosinophils

(**A**) Wright-Giemsa Staining used to quantify eosinophils (pink staining). (**B**) Quantitation of number of eosinophils per randomly chosen 20× microscopic field view. Data is presented as mean ± SEM of 5 fields per mouse from at least 3 mice per group. (**C**) Quantitation of eotaxin-1 (*Ccl11*) mRNA expression by qPCR relative to *18S*. N-values left to right: *Alb-cre*: n = 5, 5, 8, 6; *Krt19-cre*: n = 3, 4, 4, 6; *Pdgfrb-cre*: n = 3, 3, 4, 8. (**D**) Schematic illustrating the role of fibroblasts and hepatocytes in recruiting eosinophils through the IL-13

induced expression of eotaxin-1. (Note) All scale bars 100 μm; Arrows point to bile ducts; p*<0.05, p**<0.01, p***<0.001, p****<0.0001.

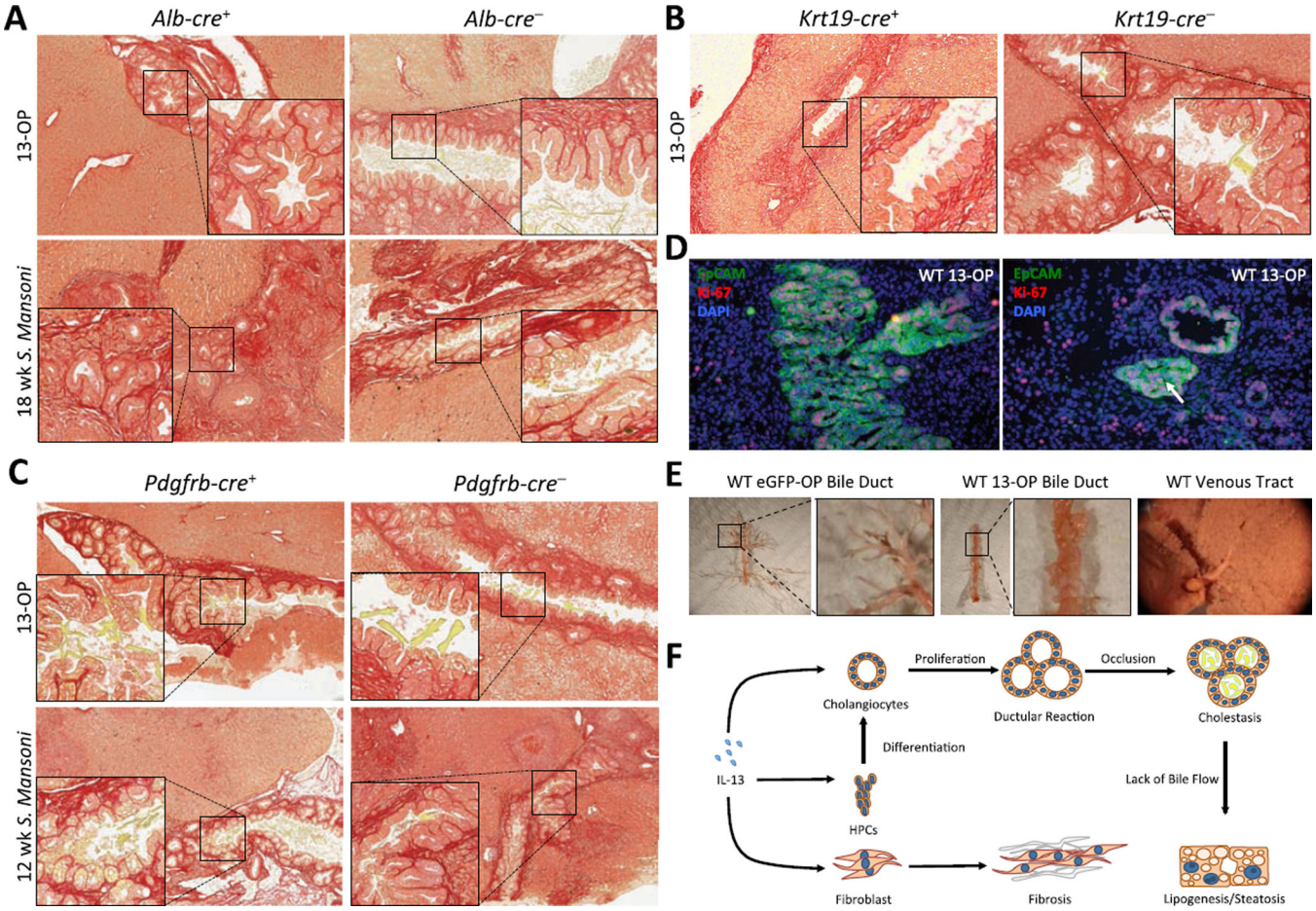

Figure 7. IL-13 Driven DR Initiates Ductal Cholestasis Independently from Fibrosis

PSR staining visualizing fibrotic deposition and highlighting the accumulation of yellow cholesterol crystals in (**A**) *Alb-cre*$^{-}$, (**B**) *Krt19-cre*$^{-}$, and (**C**) both *Pdgfrb-cre*$^{-}$ and *Pdgfrb-cre*$^{+}$ mice. (**D**) EpCAM and Ki-67 co-staining highlighting bile ducts in 13-OP mice that proliferate to the point of occlusion (arrow). (**E**) Resin casting of biliary trees from WT and 13-OP mice demonstrating a truncated biliary tree in 13-OP treated mice as a result of proliferation- induced ductal occlusion. (**F**) Schematic illustrating the role of DR in inducing cholestasis by occlusion of large branching ducts, and subsequent induction of a pro-lipogenic program within hepatocytes. (Note) All scale bars 100 μm; Please also see Figure S6.